

HYDRODYNAMICS AT RHIC*

PASI HUOVINEN

School of Physics and Astronomy, University of Minnesota
Minneapolis, MN 55455, USA

(Received April 11, 2002)

The hydrodynamical models used to describe the evolution of heavy-ion collisions are briefly reviewed and their results compared with recent RHIC data.

PACS numbers: 25.75.-q, 25.75.Ld

1. Introduction

Hydrodynamical models have certain advantages over transport model calculations in describing heavy ion collisions. One of the most important is that, once the equation of state and initial conditions of the matter are specified, the evolution of the system is determined. No knowledge of the underlying microscopic processes is required. This is especially important when studying the predicted phase transition from hadronic to partonic degrees of freedom (and *vice versa*) — a process for which details are still unknown.

The hydrodynamical description is relatively simple and fulfills the conservation laws without additional constraints. The use of familiar concepts like temperature, pressure and flow velocity also provides an intuitive and transparent picture of the evolution. The price to be paid for these advantages is a set of bold assumptions: local kinetic and chemical equilibrium and lack of dissipation. This set of assumptions may or may not be valid in such a small system as that formed in a heavy ion collision.

In a hydrodynamical description the evolution is assumed to proceed as follows: In the initial collision a large fraction of the kinetic energy of the colliding nuclei is used to create many secondary particles in a small volume. These particles will collide with each other sufficiently often to reach a state of local thermal equilibrium. When the system has reached local equilibrium

* Presented at the Cracow Epiphany Conference on Quarks and Gluons in Extreme Conditions, Cracow, Poland, January 3-6, 2002.

it is characterized by the fields of temperature, $T(x)$, chemical potentials associated with conserved charges, $\mu_i(x)$, and flow velocity, $u^\mu(x)$. The evolution of these fields is then determined by the hydrodynamical equations of motion until the system is so dilute that the assumption of local thermal equilibrium breaks down and the particles begin to behave as free particles instead.

The numerical solution of hydrodynamical equations of motion in all three spatial dimensions is a tedious problem. In most approaches some approximate symmetry is applied to reduce the number of spatial dimensions where numerical solution is needed to two or one.

In the so-called Bjorken model [1] the main idea is the boost invariance of the longitudinal flow. The longitudinal flow is assumed to be given by $v_z = z/t$ at all times. This leads to particularly simple solutions of the equations of motion since the longitudinal expansion can be solved analytically. Also it is sufficient to solve the equations of motion in the transverse plane at $z = 0$ since the solution is independent of the boosts along the beam axis. The obvious drawback in this approximation is that the observables are independent of rapidity.

In central collisions of spherical nuclei the expansion can be simplified by assuming cylindrical symmetry. Of course this symmetry can not be applied to non-central collisions where the shape of the source has a crucial role in the buildup of elliptic anisotropy.

2. Hydrodynamical models

2.1. The basics¹

Hydrodynamics is basically an application of conservation laws. The local conservation of energy and momentum and any other conserved four-currents j_i^μ , $i = 1, \dots, n$ are expressed by

$$\partial_\mu T^{\mu\nu} = 0 \quad \text{and} \quad \partial_\mu j_i^\mu = 0,$$

respectively, where $T^{\mu\nu}$ is energy momentum tensor. Without any additional constraints these $4 + n$ (n is the number of conserved currents) equations contain $10 + 4n$ unknown variables. The simplest and most commonly used approach to close this system of equations is the ideal fluid approximation which reduces the number of unknown variables to $5 + n$.

In the ideal fluid approximation the energy momentum tensor of the kinetic theory,

$$T^{\mu\nu} = \int \frac{d^3\mathbf{p}}{(2\pi)^3 E} p^\mu p^\nu f(x, \mathbf{p}),$$

¹ For a more detailed discussion see Ref. [2].

and currents j_i are supposed to have forms

$$T^{\mu\nu} = (\varepsilon + p)u^\mu u^\nu - pg^{\mu\nu} \quad \text{and} \quad j_i^\mu = n_i u^\mu,$$

where ε , p and n_i are energy density, pressure and number density of charge i in the local rest frame of the fluid, and u^μ is the flow four-velocity of the fluid. In other words all dissipative effects, such as viscosity and heat conductivity, are assumed to be zero and the fluid is always in perfect local kinetic equilibrium. The additional equation needed to close the system of equations is provided by the equilibrium Equation of State (EoS) of the matter, which connects the pressure to the densities: $P = P(\varepsilon, n_i)$.

In principle it is possible to include small deviations from local thermal equilibrium by including dissipative effects, but in practice relativistic viscous hydrodynamics is very difficult to implement and has not yet been done [2]. For preliminary results and estimates of the effects of viscosity, see Ref. [3].

2.2. Equation of state

The present results from lattice QCD calculations point to a phase transition from hadronic to partonic degrees of freedom at a temperature $T_c \approx 155\text{--}175$ MeV, but the order of the phase transition is still uncertain [4]. So far no nuclear Equation of State (EoS) based on lattice results has been employed in hydrodynamical calculations, mostly because lattice calculations are available only at zero net baryon density.

The usual way to construct an EoS is to use the EoS of a hadron gas at low temperatures and the EoS of an ideal parton gas with a bag constant at temperatures above the critical temperature T_c (see *e.g.* Ref. [5]). The EoS of an interacting hadron gas is approximated by the EoS of an ideal resonance gas with resonances up to 1.5–2 GeV mass. It is known that the inclusion of higher-lying resonances mimics interactions between hadrons well in temperatures up to the pion mass [6], but there is no reliable way to check whether this holds at higher temperatures [5]. The phase boundary is determined by using the Gibbs criteria. A first order phase transition between the hadronic and partonic phases is achieved by connecting the EoSs with the Maxwell construction.

This procedure is thermodynamically consistent and the EoS both above and below the phase transition temperature is based on well established models. However, one of its disadvantages is that it is not possible to determine the phase transition temperature and latent heat independently. To circumvent this drawback Teaney *et al.* [7] took only the speed of sound, $c_s = \sqrt{\partial p / \partial \varepsilon}$, from the bag model EoS and made the critical temperature and the latent heat explicit parameters of their model.

Constructing an EoS with a second order phase transition or crossover between the phases when only the EoSs of the separate phases are known is nontrivial. To achieve this in a consistent way Zschesche *et al.* [8] constructed a family of EoSs based on a parametrized σ - ω model. By changing the values of the parameters they were able to create two EoSs with a first order phase transition but different latent heats and an EoS with a crossover phase transition. Strictly speaking these EoSs do not contain a deconfinement phase transition but a chiral phase transition. However the EoS below and above phase transition temperature is very similar to the more conventional constructions explained above.

2.3. Initialization

Local thermal equilibrium is one of the assumptions of a hydrodynamical model; the model itself does not specify the mechanism that leads to an equilibrated state. Since at RHIC energies the initial particle production is definitely not an adiabatic process, hydrodynamics can not be used to describe the initial collision. The hydrodynamical evolution must begin at a sufficient time after the initial collision when the system has had time to reach thermal equilibrium. The initial state of the system, *i.e.* the density distributions and flow velocities at the beginning of the hydrodynamic evolution, are not given by the model either but must be given as external input.

When a boost invariant expansion is assumed, the choice of an initial state is reduced to a choice of transverse density and velocity profiles. A simple approach is to fix the value of the entropy to reproduce the observed final particle multiplicity and to distribute it on the transverse plane assuming a constant density profile within the radius of the colliding nuclei using a Fermi function to smooth the edges of the system. However, this approach cannot be applied to non-central collisions. One must also remember that since it is the local pressure gradients which drive the development of transverse flow and the evolution of the system, the details of flow are sensitive to the details of the initial distributions [9]. In the same way the final anisotropies are proportional to the deformation of the source and additional constraints to the initial distributions are required.

It is known that up to SPS energies the multiplicity scales with the number of nucleons participating in the collision [10]. On the other hand, in the high energy limit one expects the individual parton-parton collisions to contribute equally to primary particle production and therefore, the multiplicity should scale with the number of binary collisions [11]. Therefore, it is natural to initialize the system using a localized version of these approaches: to assume that the density is proportional either to the number of partici-

pants or to the number of binary collisions per unit area in the transverse plane. Both approaches, or a combination of them can be used to fix the initial entropy or energy density; a comparison was made in Ref. [12]. The initial transverse flow velocity is customarily assumed to be zero, although pre-equilibrium density gradients might lead to small, but finite, transverse flow velocities at the time of thermalization.

If the assumption of boost invariance is relaxed the choice of initial state becomes considerably more complicated. There are few constraints for the flow velocity profile or the longitudinal density distributions. The choice of a particular parametrization and the values of the parameters is largely based on trial and error — tuning the model until a reasonable fit to experimental rapidity distributions is achieved. Even for the same EoS there are several possible initial states which lead to an acceptable reproduction of the data [13]. For a sample of initial profiles used successfully see Refs. [5, 14–16].

An alternative approach to determine the initial state is to use some other model to calculate it. For example, event generators [17] or perturbative QCD (pQCD) calculations [18] have been used for this purpose. Even if these approaches increase the predictive power of hydrodynamics, thermalization is still an additional assumption.

2.4. Freeze-out

At some point in the evolution particles will begin to behave as free particles instead of a fluid and the hydrodynamical description breaks down. When and where that happens is not given by hydrodynamics but must be included as an external input. The conventional approach is to assume this to take place as a sudden transition from local thermal equilibrium to free streaming when the mean free path of the particles becomes larger than the system size, or when the expansion rate of the system is larger than the collision rate between particles. Finding where these conditions are fulfilled is a nontrivial problem. Since the mean free path is strongly dependent on temperature the usual approximation assumes that the freeze-out takes place on a hypersurface where temperature (or energy density) has a chosen freeze-out value. This temperature is of the order of the pion mass, but its exact value is largely a free parameter which can be chosen to fit the data. In Pb + Pb collisions at the SPS the values of freeze-out temperatures vary between 100 and 140 MeV in different calculations [19].

These values are somewhat smaller than the $T \sim 160$ MeV freeze-out temperatures obtained using thermal models to fit the particle abundances at final state [20]. This can be understood by noticing that the former approaches assume kinetic equilibrium while the thermal models assume chemical equilibrium. Since chemical equilibrium requires frequent inelas-

tic collisions, while kinetic equilibrium only requires elastic collisions, it is natural to assume that inelastic collisions cease first and chemical freeze-out occurs at higher temperatures than kinetic freeze-out. Thus the system may be in local kinetic, but not chemical, equilibrium at the later stages of its evolution. How much this would affect the EoS and whether this change in the EoS would have any observable effects in the evolution of the system is so far largely unexplored (with some early exceptions like Ref. [21]). However, first preliminary results have been shown and more are in preparation [22].

After choosing the surface where the freeze-out takes place, the thermodynamic variables characterizing the state of the fluid must be converted to spectra of observable particles. A practical way of doing this is the Cooper–Frye algorithm [23] where the invariant momentum distribution of a hadron h is given by

$$E \frac{dN}{d^3p} = \frac{g_h}{(2\pi)^3} \int_{\sigma_f} \frac{1}{\exp[(p_\mu u^\mu - \mu)/T] \pm 1} p^\mu d\sigma_\mu.$$

Here the temperature $T(x)$, chemical potential $\mu(x)$ and flow velocity $u^\mu(x)$ are the values on the decoupling surface σ_f . Besides its relative simplicity, this approach has the advantage that if the same equation of state is used on both sides of decoupling surface, both energy and momentum are conserved. However, the Cooper–Frye formula has a conceptual problem. At those areas where the freeze-out surface is spacelike, the product $p^\mu d\sigma_\mu$ may be either positive or negative, depending on the value and direction of p^μ . In other words, the number of particles freezing out on some parts of the freeze-out surface may be negative. These negative contributions are small (few per cent, see Ref. [7]) and usually ignored. More refined procedures without negative contributions have been suggested [24] but their implementation is complicated. A model using one of these refined freeze-out procedures is in preparation [25] and it will be interesting to see how large an effect the freeze-out procedure has on the final particle spectra in a full-fledged calculation.

Another way to refine the hydrodynamical freeze-out procedure is to switch from a hydrodynamical to a microscopic transport model description well within the region where hydrodynamics is supposed to be applicable [7,26]. Besides giving a better description of freeze-out, such models include the separate chemical and kinetic freeze-outs. The main drawback of such models — apart from the increased complexity — is that the region where the switch from hydro to transport description should take place is as poorly defined as kinetic freeze-out surface in ordinary hydrodynamical calculation. The educated guess employed in both Refs. [7,26] is that the switch happens immediately after hadronization.

3. Comparison with the data

3.1. Charged particle multiplicity and transverse energy

In ideal fluid hydrodynamics the final particle multiplicity is proportional to the entropy of the initial state. Thus in a certain sense multiplicity is not really a *hydrodynamical* result, but something one dials in as input. Nevertheless, when the initial state is not chosen by comparing the final result to data, but calculated from perturbative QCD as in Ref. [18], the final particle multiplicity becomes a prediction of the model.

In Ref. [18] Eskola *et al.* used the EKRT saturation model to calculate the production of minijets in the primary collisions and then converted this result to the initial state of hydrodynamic evolution. Their results for charged particle multiplicities at RHIC and LHC energies are shown in Fig. 1. The results agree well with the data measured by the PHOBOS Collaboration [27,28]. It is important to remember that no fitting or fine tuning was done to achieve this result, and that the multiplicity at $\sqrt{s_{NN}} = 200$ GeV energy was not yet measured when this calculation was done.

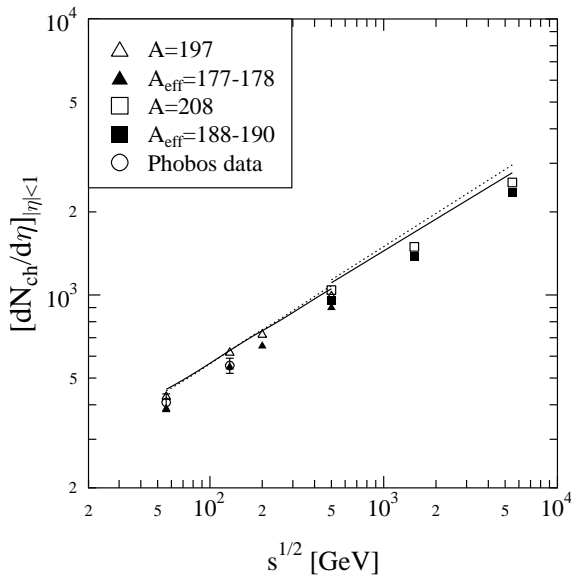


Fig. 1. Charged particle multiplicity calculated at different collision energies and compared to PHOBOS data [27] and calculations (solid and dotted lines) in Ref. [29]. $A = 197$ and 208 refer to the mass of the nuclei and A_{eff} to a finite impact parameter. Figure and calculation are from Ref. [18].

When compared with the EKRT saturation results shown in Ref. [29], which did not contain an expansion stage, one notices that hydrodynamical expansion causes only a small change in multiplicity, but the transverse energy decreases by a factor 3. However, at RHIC the calculated E_T is still 10–20 % larger than the experimental value [30].

3.2. p_T spectra

The conventional way to initialize a hydrodynamical calculation is to use experimental hadron data to fix the initial values. Depending on the details of the initialization the calculated p_T distributions can be only fits to the data or have some predictive power. In Ref. [33] the initialization is done by first choosing the initial entropy and the net baryon densities to reproduce the observed pion multiplicity and \bar{p}/p ratio in the most central collisions. Then a combination of different parametrizations mentioned in Section 2.3 and Ref. [12] is chosen to reproduce the observed multiplicity per participant as function of centrality. In this process the slopes of the spectra or the centrality dependence of the slopes are not used as an input and their calculated values can be taken as predictions.

In central collisions this initialization led to a maximum initial temperature $T_{\max} = 328$ MeV and an energy density $\varepsilon_{\max} = 21.4$ GeV/fm³ at an initial time $\tau_0 = 0.6$ fm/ c . At time $\tau = 1$ fm/ c , usually used to estimate initial energy density via Bjorken's formula [1], the corresponding average energy density is $\langle\varepsilon\rangle = 5.4$ GeV/fm³, which is consistent with experimental estimates [30].

Local chemical equilibrium is assumed to hold until kinetic freeze-out. Thus chemical and kinetic freeze-outs take place at the same temperature. Even if the pion yield is correctly reproduced in Ref. [33], it is not possible to obtain both correct proton and antiproton yields simultaneously. The authors have chosen to circumvent this problem by calculating the particle yields at hadronization temperature $T_c = T_{\text{chem}} = 165$ MeV and calculating the slopes of the p_T spectra at $T_f = 128$ MeV. Subsequently they rescale the particle yields at kinetic freeze-out to their values at chemical freeze-out by hand. The results shown here in Figs. 2 and 3 are very similar to those in Ref. [7]. Since separate chemical and kinetic freeze-out was included in the transport model description of hadronic phase of Ref. [7], one can conclude that the method applied in Ref. [33] provides a reasonable approximation.

It has been observed that around $p_T = 2$ GeV the antiproton and pion yields are roughly equal, and the slopes of the distributions suggest that the antiproton yield is *larger* than pion yield for $p_T > 2$ GeV [31]. As can be seen in Fig. 2 this phenomenon can be explained as a simple consequence of strong transverse flow. Besides giving an explanation for this so-called

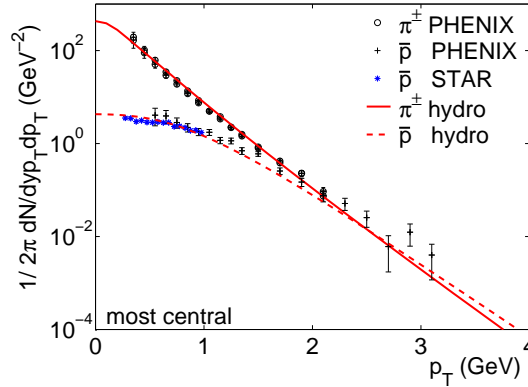


Fig. 2. Charged pion and antiproton spectra from most central Au+Au collisions at the $\sqrt{s_{NN}} = 130$ GeV as measured by the PHENIX [31] and STAR [32] Collaborations. The hydrodynamical calculation and figure are from Ref. [33].

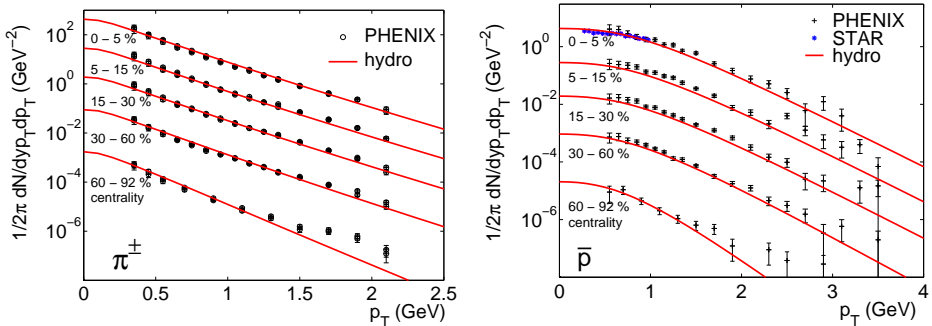


Fig. 3. Charged pion (left panel) and antiproton (right panel) spectra from Au+Au collisions at $\sqrt{s_{NN}} = 130$ GeV at various centralities as measured by the PHENIX [31] and STAR [32] Collaborations. The hydrodynamical calculation and figures are from Ref. [33].

anomalous \bar{p}/π ratio, hydrodynamical calculation provides very good fit to both pion and antiproton spectra both in central and semicentral collisions. As can be seen in Fig. 3 the deviation from the data is significant only in the most peripheral collisions.

3.3. Elliptic anisotropy

Since the initial particle production is azimuthally symmetric, azimuthal anisotropy of the final particle distributions is a signal of rescatterings among produced particles. More frequent rescattering can be expected to lead to a larger anisotropy and since hydrodynamics assumes zero mean free path

and thus an infinite scattering rate, it provides an upper limit to observable anisotropies. Anisotropy is quantified by measuring the harmonic coefficients $v_n(y, p_T; b)$ of a Fourier expansion in ϕ_p of the measured hadron spectrum $dN/(dy p_T dp_T d\phi_p)$ [34]. Anisotropy characterized by a non-zero second coefficient, v_2 , is called elliptic anisotropy or elliptic flow [35].

In Fig. 4 the centrality dependence of the elliptic anisotropy coefficient v_2 in Au + Au collisions at $\sqrt{s_{NN}} = 130$ GeV energy is shown [36]. The calculations of Refs. [7, 37] give very similar results: in central and semi-central collisions the data reaches the hydrodynamical limit and depending on the EoS and freeze-out temperature (the latter is not shown in Fig. 4) the agreement is satisfactory even close to peripheral collisions. The calculation shown in Fig. 4 was carried out using various EoSs with different latent heats [7]. The best fit to the data is obtained using an EoS with a relatively large latent heat, but when other observables are considered, the authors conclude that LH8 EoS with smaller latent heat leads to best overall description of data.

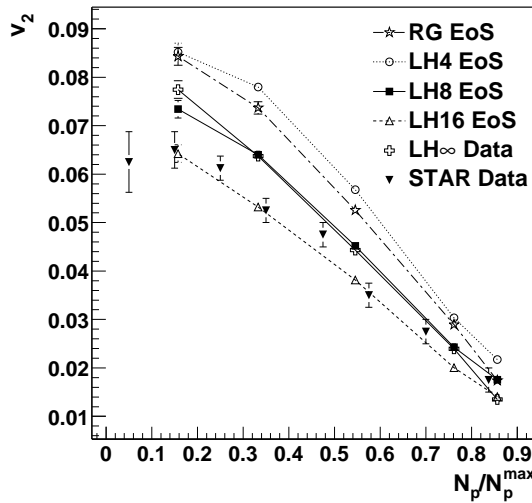


Fig. 4. Elliptic anisotropy coefficient v_2 for charged particles at RHIC as a function of the number of participants (relative to the maximum) as measured by the STAR Collaboration [36] and calculated using different equations of state [7]. The label RG corresponds to a resonance gas EoS without a phase transition. The number in other labels describes the latent heat. The figure is from Ref. [7].

In a hydrodynamical model the final anisotropy is proportional to the initial deformation of the source. The deformation as a function of impact parameter depends on the particular parametrization applied but, as shown in Ref. [12], when the anisotropy is averaged over all momenta and central-

ity is expressed as a fraction of the total multiplicity, differences between parametrizations even out. Thus the result shown in Fig. 4 is independent of the particular parametrization.

The p_T differential anisotropy, $v_2(p_T)$, for pions and for the sum of protons and antiprotons [38] depicted in Fig. 5 also shows clear hydrodynamical behavior. As predicted² in Ref. [39], the heavier the particle, the smaller the anisotropy at low p_T . So far there are no published data regarding the p_T differential anisotropy of strange particles so whether they also obey this rule remains to be seen. The identified particle data is so far limited to the low p_T region shown in Fig. 5. The p_T differential anisotropy of negative hadrons [40] follows the hydrodynamical calculations up to transverse momenta $p_T \leq 1.5$ –2 GeV (not shown) where the anisotropy saturates. The deviation can be understood as a sign of incomplete thermalization of high- p_T particles.

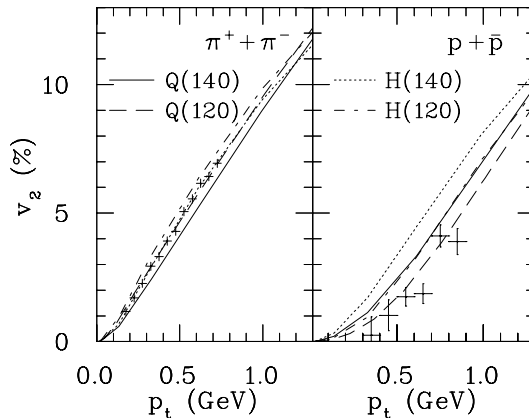


Fig. 5. p_T differential elliptic anisotropy of pions (left panel) and protons + antiprotons (right panel) in minimum bias collisions as measured by the STAR Collaboration [38] and calculated using different equations of state and freeze-out temperatures [39]. The letters Q and H in the labels stand for an EoS with a first order phase transition and a hadron gas EoS without a phase transition, respectively. Numbers in parentheses stand for the freeze-out temperature in MeV.

It is well known that the changes in the EoS can be compensated by changing the initial state and freeze-out temperature (see *e.g.* Ref. [13]). A remarkable feature of Fig. 5 is that changes in the EoS affect the anisotropy of both pions and nucleons in the same way — a stiffer EoS leads to a larger anisotropy at low values of p_T — but a change in freeze-out temperature changes the pion and nucleon anisotropies in opposite directions. A lower

² A similar result was later obtained in Ref. [7].

freeze-out temperature leads to a larger anisotropy for pions but to a smaller anisotropy for nucleons (for further discussion, see Ref. [39]). This may provide an additional method of constraining possible equations of state and freeze-out temperatures.

In the studies mentioned above the expansion was assumed to be boost invariant. Judging by the measured rapidity distributions [41], this is a reasonable assumption close to midrapidity, but it makes it impossible to make any statements about the rapidity dependence of any variable. To study the rapidity dependence of the elliptic anisotropy the assumption of boost invariance was relaxed and the calculation was done using a genuinely three dimensional model in Ref. [16]. When compared to the excellent agreement with the data in Figs. 4 and 5, the result depicted in Fig. 6 [16] may look less satisfactory. The data [42] reaches the hydrodynamical value only around midrapidity. On the other hand, even this result reproduces the data within a one to two units of pseudorapidity wide window. This area already contains most of the produced particles. It is also worth remembering that anisotropy in hydrodynamical models depends strongly on the initial shape of the system. The initialization used in Ref. [16] is relatively simple and more sophisticated initialization may lead to better fit to the data. Therefore, it is premature to conclude based on this data and calculation alone that thermalization is reached only at midrapidity

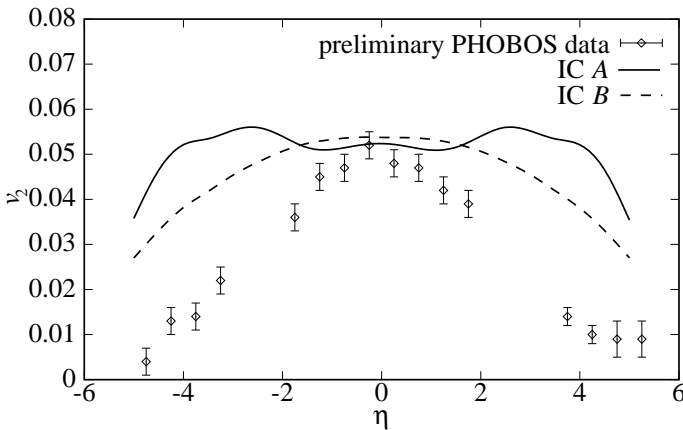


Fig. 6. Pseudorapidity dependence of elliptic anisotropy for charged particles in minimum bias collisions at $\sqrt{s_{NN}} = 130$ GeV energy. The figure and calculations are from Ref. [16] and the experimental data from Ref. [42]. Dashed and dotted lines correspond to different initializations of the model, see Ref. [16].

3.4. Two particle correlations

Two particle momenta correlations, known as HBT interferometry, provide a method to study the space-time structure of the emitting source [43]. It has been predicted that a first order phase transition would lead to unusually large HBT-radii [44]. However, comparisons of calculations [8,33,45] with data [46,47] have lead to the so-called *HBT-puzzle*: All calculations give a ratio of HBT-radii $R_{\text{out}}/R_{\text{side}}$ larger than one, but the experimental value is of order one. The calculated values of R_{out} are also larger and, with the exception of Ref. [45], values of R_{side} are smaller than observed.

It has been suggested that the solution to this puzzle lies primarily in the description of freeze-out [33]. This is doubtful since even calculations where the hadronic phase is described using a transport model cannot describe the data correctly [45], even though this kind of freeze-out description should be more reliable. Some other theoretical uncertainties, such as the order of the phase transition and choice of freeze-out temperature, were addressed in Ref. [8]. As shown in Fig. 7, it was found that the freeze-out temperature has quite a small effect on the radii nor were any of the tested EoSs (EoS with strong first order, weak first order and cross-over phase transitions) able to provide an acceptable reproduction of the data. Since the EoS with a smooth cross-over phase transition (CI in Fig. 7) is closest to the data, it is possible to claim that HBT measurements favour an EoS with smooth cross-over. This is particularly interesting since, as argued in Section 3.3, elliptic

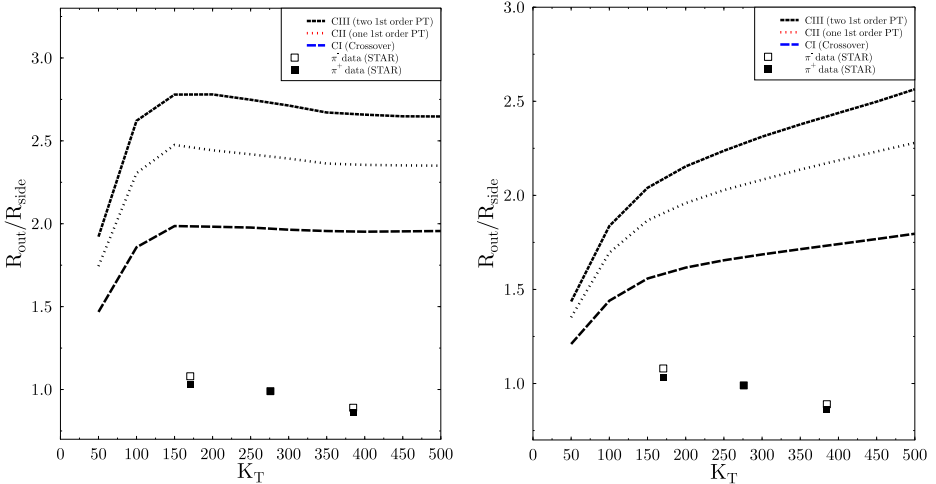


Fig. 7. $R_{\text{out}}/R_{\text{side}}$ as function of K_T for $T_f = 130$ (left panel) and 80 MeV (right panel) using different equations of state compared to STAR data [46]. The calculation and figures are from Ref. [8].

anisotropy seems to favour a moderately strong first order phase transition. The explanation to this seemingly contradictory behaviour, as well as to the entire HBT-puzzle, is still unknown at present.

4. Summary

Hydrodynamical models have been very successful in explaining the single particle RHIC data at low p_T . The p_T spectra and anisotropies in central and semicentral collisions are well reproduced for $p_T \leq 1.5\text{--}2$ GeV and the \bar{p}/π ratio at $p_T \sim 2$ GeV/ c has a simple explanation due to flow. Especially impressive has been how hydrodynamics is able to create simultaneously elliptic anisotropy of negative hadrons which is large enough and anisotropy of protons which is small enough to fit the data. If one considers solely this data the collision system behaves like a thermal system.

However, the reproduction of the HBT-radii has been unsuccessful so far. It is unclear whether one should refine the final freeze-out process, hadronization process, or initial state to reach an acceptable description of the data. Especially puzzling is the fact that the HBT-radii seem to favour a relatively stiff equation of state with a crossover phase transition, whereas elliptic anisotropy of protons favours a soft equation of state with a first order phase transition.

I thank the organizers for the invitation to this conference and P.J. Ellis, J.I. Kapusta and A. Muronga for careful readings of the manuscript. This work was supported by the US Department of Energy grant DE-FG02-87ER40328.

REFERENCES

- [1] J.D. Bjorken, *Phys. Rev.* **D27**, 140 (1983).
- [2] D.H. Rischke, *Lect. Notes Phys.* **516**, 21 (1999).
- [3] A. Muronga, *Phys. Rev. Lett.* **88**, 062302 (2002); `nuc1-th/0105046`.
- [4] F. Karsch, *Nucl. Phys.* **A698**, 199 (2002).
- [5] J. Sollfrank, P. Huovinen, M. Kataja, P.V. Ruuskanen, M. Prakash, R. Venugopalan, *Phys. Rev.* **C55**, 392 (1997).
- [6] R. Venugopalan, M. Prakash, *Nucl. Phys.* **A546**, 718 (1992).
- [7] D. Teaney, J. Lauret, E.V. Shuryak, `nuc1-th/0110037`.
- [8] D. Zschesche, S. Schramm, H. Stocker, W. Greiner, `nuc1-th/0107037`.
- [9] A. Dumitru, D. H. Rischke, *Phys. Rev.* **C59**, 354 (1999).
- [10] M.M. Aggarwal *et al.* [WA98 Collaboration], *Eur. Phys. J.* **C18**, 651 (2001).

- [11] K. Kajantie, P.V. Landshoff, J. Lindfors, *Phys. Rev. Lett.* **59**, 2527 (1987); K.J. Eskola, K. Kajantie, J. Lindfors, *Nucl. Phys.* **B323**, 37 (1989).
- [12] P.F. Kolb, U.W. Heinz, P. Huovinen, K.J. Eskola, K. Tuominen, *Nucl. Phys.* **A696**, 197 (2001).
- [13] P. Huovinen, P.V. Ruuskanen, J. Sollfrank, *Nucl. Phys.* **A650**, 227 (1999).
- [14] U. Ornik, M. Plumer, B. R. Schlei, D. Strottman, R.M. Weiner, *Phys. Rev.* **C54**, 1381 (1996).
- [15] J. Sollfrank, P. Huovinen, P.V. Ruuskanen, *Eur. Phys. J.* **C6**, 525 (1999).
- [16] T. Hirano, *Phys. Rev.* **C65**, 011901 (2002).
- [17] B.R. Schlei, D. Strottman, *Phys. Rev.* **C59**, 9 (1999).
- [18] K.J. Eskola, P.V. Ruuskanen, S.S. Rasanen, K. Tuominen, *Nucl. Phys.* **A696**, 715 (2001).
- [19] D.H. Rischke, *Nucl. Phys.* **A698**, 153 (2002).
- [20] J. Cleymans, K. Redlich, *Phys. Rev.* **C60**, 054908 (1999).
- [21] H. Bebie, P. Gerber, J.L. Goity, H. Leutwyler, *Nucl. Phys.* **B378**, 95 (1992); M. Kataja, P.V. Ruuskanen, *Phys. Lett.* **B243**, 181 (1990).
- [22] T. Hirano, K. Tsuda, nucl-th/0202033; D. Teaney, nucl-th/0204023.
- [23] F. Cooper, G. Frye, *Phys. Rev.* **D10**, 186 (1974).
- [24] K.A. Bugaev, *Nucl. Phys.* **A606**, 559 (1996); K.A. Bugaev, M.I. Gorenstein, nucl-th/9903072; V.K. Magas *et al.*, *Nucl. Phys.* **A661**, 596 (1999).
- [25] L.P. Csernai, private communication.
- [26] S.A. Bass, A. Dumitru, *Phys. Rev.* **C61**, 064909 (2000).
- [27] B.B. Back *et al.* [PHOBOS Collaboration], *Phys. Rev. Lett.* **85**, 3100 (2000).
- [28] B.B. Back *et al.* [PHOBOS Collaboration], *Phys. Rev. Lett.* **88**, 022302 (2002).
- [29] K.J. Eskola, K. Kajantie, P.V. Ruuskanen, K. Tuominen, *Nucl. Phys.* **B570**, 379 (2000).
- [30] K. Adcox *et al.* [PHENIX Collaboration], *Phys. Rev. Lett.* **86**, 3500 (2001).
- [31] J. Velkovska [PHENIX Collaboration], *Nucl. Phys.* **A698**, 507 (2002).
- [32] C. Adler *et al.* [STAR Collaboration], *Phys. Rev. Lett.* **87**, 262302 (2001).
- [33] U.W. Heinz, P.F. Kolb, hep-ph/0111075.
- [34] S. Voloshin, Y. Zhang, *Z. Phys.* **C70**, 665 (1996).
- [35] J.Y. Ollitrault, *Phys. Rev.* **D46**, 229 (1992).
- [36] K.H. Ackermann *et al.* [STAR Collaboration], *Phys. Rev. Lett.* **86**, 402 (2001).
- [37] P.F. Kolb, P. Huovinen, U.W. Heinz, H. Heiselberg, *Phys. Lett.* **B500**, 232 (2001).
- [38] C. Adler *et al.* [STAR Collaboration], *Phys. Rev. Lett.* **87**, 182301 (2001).
- [39] P. Huovinen, P.F. Kolb, U.W. Heinz, P.V. Ruuskanen, S.A. Voloshin, *Phys. Lett.* **B503**, 58 (2001).
- [40] R.J. Snellings [STAR Collaboration], *Nucl. Phys.* **A698**, 193 (2002).
- [41] B.B. Back *et al.* [PHOBOS Collaboration], *Phys. Rev. Lett.* **87**, 102303 (2001).

- [42] I.C. Park *et al.* [PHOBOS Collaboration], *Nucl. Phys.* **A698**, 564 (2002).
- [43] U.W. Heinz, B.V. Jacak, *Ann. Rev. Nucl. Part. Sci.* **49**, 529 (1999);
U.A. Wiedemann, U.W. Heinz, *Phys. Rep.* **319**, 145 (1999).
- [44] D.H. Rischke, M. Gyulassy, *Nucl. Phys.* **A608**, 479 (1996).
- [45] S. Soff, S.A. Bass, A. Dumitru, *Phys. Rev. Lett.* **86**, 3981 (2001); S. Soff,
[hep-ph/0202240](#).
- [46] C. Adler *et al.* [STAR Collaboration], *Phys. Rev. Lett.* **87**, 082301 (2001).
- [47] K. Adcox *et al.* [PHENIX Collaboration], [nucl-ex/0201008](#).